Monthly Notices of the ROYAL ASTRONOMICAL SOCIETY

MNRAS **454,** 1620–1633 (2015) doi:10.1093/mnras/stv2095

Dust processing in elliptical galaxies

Hiroyuki Hirashita,[1★] Takaya Nozawa,[2] Alexa Villaume[3] and Sundar Srinivasan[1]

[1] *Institute of Astronomy and Astrophysics, Academia Sinica, PO Box 23-141, Taipei 10617, Taiwan*
[2] *National Astronomical Observatory of Japan, Mitaka, Tokyo 181-8588, Japan*
[3] *Department of Astronomy and Astrophysics, University of California, Santa Cruz, CA 95064, USA*

Accepted 2015 September 7. Received 2015 September 3; in original form 2015 August 4

ABSTRACT

We reconsider the origin and processing of dust in elliptical galaxies. We theoretically formulate the evolution of grain size distribution, taking into account dust supply from asymptotic giant branch (AGB) stars and dust destruction by sputtering in the hot interstellar medium (ISM), whose temperature evolution is treated by including two cooling paths: gas emission and dust emission (i.e. gas cooling and dust cooling). With our new full treatment of grain size distribution, we confirm that dust destruction by sputtering is too efficient to explain the observed dust abundance even if AGB stars continue to supply dust grains, and that, except for the case where the initial dust-to-gas ratio in the hot gas is as high as ∼0.01, dust cooling is negligible compared with gas cooling. However, we show that, contrary to previous expectations, cooling does not help to protect the dust; rather, the sputtering efficiency is raised by the gas compression as a result of cooling. We additionally consider grain growth after the gas cools down. Dust growth by the accretion of gas-phase metals in the cold medium increase the dust-to-gas ratio up to $\sim 10^{-3}$ if this process lasts $\gtrsim 10/(n_{\rm H}/10^3\ {\rm cm^{-3}})$ Myr, where $n_{\rm H}$ is the number density of hydrogen nuclei. We show that the accretion of gas-phase metals is a viable mechanism of increasing the dust abundance in elliptical galaxies to a level consistent with observations, and that the steepness of observed extinction curves is better explained with grain growth by accretion.

Key words: methods: analytical – dust, extinction – galaxies: elliptical and lenticular, cD – galaxies: evolution – galaxies: ISM.

1 INTRODUCTION

In the nearby Universe, elliptical galaxies are known to have little ongoing star formation activity. However, elliptical galaxies are not completely devoid of gas: they are also known to have hot X-ray-emitting halo gas (e.g. O'Sullivan, Forbes & Ponman 2001) and cold gas (e.g. Wiklind, Combes & Henkel 1995). Moreover, dust is detected for a large (>50 per cent) fraction of elliptical galaxies by optical extinction (e.g. Goudfrooij et al. 1994a; van Dokkum & Franx 1995; Ferrari et al. 1999; Tran et al. 2001) or far-infrared (FIR) emission (e.g. Knapp et al. 1989). Dust mass is estimated to be 10^4–10^5 $M_\odot$ from the reddening in the optical (Goudfrooij et al. 1994a). The dust mass estimated from FIR dust emission tends to be even larger ($\sim 10^5$–10^7 $M_\odot$; e.g. Leeuw et al. 2004; Temi et al. 2004). The existence of dust is also important in determining the chemical properties of the cold gas through dust-surface reactions and freeze-out of molecules on to the dust (Fabian, Johnstone & Daines 1994; Voit & Donahue 1995). In spite of such an important role of dust, the origin of dust in elliptical galaxies is still being debated, and there is no clear theoretical explanation for the total amount of dust there.

Because the stellar population is dominated by old stars whose ages are comparable to the cosmic age, the dust is predominantly supplied by asymptotic giant branch (AGB) stars in elliptical galaxies. However, the supplied dust is quickly destroyed by sputtering in the X-ray-emitting hot gas. This destruction is so efficient that the observed dust mass cannot be explained by the dust abundance achieved by the balance between the supply from AGB stars and the destruction (e.g. Patil et al. 2007). Therefore, the existence of such an 'excessive' amount of dust has long been a mystery.

Some authors argue that the dust existing in elliptical galaxies is possibly injected from outside via the merging or accretion of external galaxies (Forbes 1991; Temi et al. 2004; Fujita et al. 2013). The lack of correlation between dust FIR luminosity and stellar luminosity is also taken as evidence of external origin of dust (Temi, Brighenti & Mathews 2007); however, this argument implicitly assumes that the existing dust is tightly related to the stellar dust production activity. If dust is processed by mechanisms not related to stars, it may be natural that we do not find a correlation between

★ E-mail: hirashita@asiaa.sinica.edu.tw

dust emission and stellar luminosity. In particular, dust may grow through the accretion of gas-phase metals in the cold gas, and this dust growth is suggested to be the most efficient mechanism of dust mass increase in nearby galaxies (e.g. Dwek 1998; Hirashita 1999; Zhukovska, Gail & Trieloff 2008; Inoue 2011; Mattsson & Andersen 2012; Asano et al. 2013a; de Bennassuti et al. 2014; Rémy-Ruyer et al. 2014). Indeed, Fabian et al. (1994) and Voit & Donahue (1995) pointed out a possibility of dust reformation in a cooling flow. More recently, Martini, Dicken & Storchi-Bergmann (2013) also suggested the importance of accretion in maintaining the dust abundance to a level consistent with observations by analogy with the Milky Way. Since the efficiency of dust growth is not necessarily related to the stellar properties of elliptical galaxies, the lack of correlation between dust and stellar emissions does not necessarily mean the external origin of dust.

The interstellar dust is not only passively processed in the ISM, but could also actively regulate the physical state of the ISM, since dust is able to radiate away the energy obtained by collisions with gas particles. This is one of the most important cooling paths of the hot ISM, and referred to as dust cooling. Mathews & Brighenti (2003) argued that dust cooling could occur faster than the dynamical time in the galactic potential and thus possibly enable the dust to survive against sputtering. However, they did not treat the dust supply from AGB stars consistently, and they assumed a relatively high initial dust-to-gas ratio ($\sim$0.01, which is comparable to the dust-rich ISM seen in the Milky Way) in the hot gas. Since there has been some advance in the theoretical understanding of dust production in AGB stars (Ferrarotti & Gail 2006; Ventura et al. 2012), it is worth reconsidering their models using the new knowledge about the dust yield. Moreover, since Mathews & Brighenti (2003) assumed a single grain size for dust cooling, it would be interesting to calculate the evolution of grain size distribution: indeed, the grain size distribution is of fundamental importance in comparison with observed extinction curves as we argue below. The rates of sputtering and dust cooling also depend on the grain size distribution (Dwek 1987; Nozawa, Kozasa & Habe 2006).

The evolution of dust is also linked to active galactic nucleus (AGN) activities in elliptical galaxies. Temi et al. (2007) proposed the transportation of dust from dust reservoirs in the central regions to explain the extended dust emission in elliptical galaxies (see also Mathews et al. 2013). In this context, the origin, production, and survival of dust are important in clarifying the origin of the dust reservoirs. As mentioned above, dust may also contribute to cooling. The cool gas that falls into the centre may fuel the AGN (e.g. Werner et al. 2014), which in turn works as a heating source and reforms the hot gas (Ciotti & Ostriker 2001). Recently, Valentini & Brighenti (2015) pointed out that the AGN feedback could also enhance cooling locally through compression.

In this paper, we focus on the processing of dust in elliptical galaxies, both in the hot and cold gas components. In order to avoid complexity arising from the AGN feedback, we do not treat the supply of hot gas through the feedback but start the calculation given the pre-existing hot gas. Instead, we do treat cooling of the gas in a consistent manner with the dust supply and destruction in the hot gas. Since dust cooling and dust destruction depend on the grain size distribution, we fully take the evolution of grain size distribution into account. We additionally consider the impact of dust growth in the cooled gas not only on the dust amount, but also on the grain size distribution. Through the modelling of the above processes, we will be able to clarify the evolution and survival of dust in a cooling cycle of the ISM in elliptical galaxies.

We emphasize that the treatment of grain size distribution is one of the most important features in our modelling. Indeed, there is an observational clue to the grain size distribution, which enables us to test our results. The wavelength dependence of extinction, the so-called extinction curve, is investigated for a statistical number ($\gtrsim$10) of elliptical galaxies: Goudfrooij et al. (1994b) showed that the ratio of total to selective extinction R_V, which is a measure of the flatness of optical extinction curve, tends to be smaller ($R_V = 2.1$–3.3) than the mean value of the Milky Way extinction curves (3.1; e.g. Pei 1992; Weingartner & Draine 2001; Draine 2003; Fitzpatrick & Massa 2007; Nozawa & Fukugita 2013). This implies that the typical grain size is smaller in the elliptical galaxies than in the Milky Way. Patil et al. (2007) obtained a similar range ($R_V = 2.03$–3.46) for 11 elliptical galaxies. These extinction curves can be used to examine the evolution of grain size distributions through various processes in the ISM.

The paper is organized as follows: we explain our models for the basic processes of dust evolution in the hot ISM in Section 2. We show the results in Section 3. We additionally consider dust processing in the cold ISM, focusing on dust growth, in Section 4. In Section 5, some predicted features of the models such as dust abundance and extinction curves are compared with observations. Finally, we conclude in Section 6.

2 PROCESSING IN THE HOT ISM

We explain the method of calculating the evolution of dust grain size distribution in the hot ISM in an elliptical galaxy. Our models are composed of dust supply by AGB stars and dust destruction by sputtering. Cooling of the hot gas by dust thermal emission and gas line emission is also calculated in a consistent manner with the evolution of dust grain size distribution. To avoid the complexity arising from dynamical evolution determined by the gravitational field and the AGN heating, we only consider the evolution of a local 'fluid element' of the ISM without modelling the global dynamics. The simplicity of this approach enables us to focus on dust processing which is determined by the local environment where the dust resides.

2.1 Evolution of grain size distribution

The grain size distribution at time t is defined so that $n(a, t)\,\mathrm{d}a$ is the number density of grains in the range of grain radii between a and $a + \mathrm{d}a$. The time t is measured from the onset of dust processing in the hot gas (t is *not* the age of the galaxy). As mentioned above, we focus on a local region without considering the global gas and dust distributions within the galaxy. We also assume that the gas and dust are well coupled (i.e. once dust is injected into a certain gas element, that dust stays in the same element without any displacement; in other words, the Lagrangian trajectories of gas and dust are the same). Under these assumptions, the evolution of grain size distribution in the hot gas is described as

$$\frac{\partial n(a,\,t)}{\partial t} + \frac{\partial}{\partial a}[\dot{a}n(a,\,t)] = S(a,\,t) + n(a,\,t)\frac{\mathrm{d}\ln\rho_{\mathrm{gas}}}{\mathrm{d}t}, \tag{1}$$

where $\dot{a} = \mathrm{d}a/\mathrm{d}t$ is the changing rate of grain radius by sputtering ($\dot{a}$ is negative; see Section 2.3), $S(a, t)$ is the source term due to the dust production by AGB stars (Section 2.2), and ρ_{gas} is the gas mass density. The last term in equation (1) is the increase of the grain number density by the change of the background gas density (Appendix A): as formulated in Section 2.4, we consider the change of gas density by cooling. We give the number density of hydrogen nuclei, $n_{\rm H}$, as an input parameter, and the relation between $n_{\rm H}$ and $\rho_{\rm gas}$ is given by

$$\rho_{\rm gas} = \mu m_{\rm H} n_{\rm H}, \tag{2}$$

where $m_{\rm H}$ is the mass of hydrogen atom, and μ is the mean weight of the gas per hydrogen (we adopt $\mu = 1.4$).

Since we are often interested in the grain mass, we introduce the grain size distribution per unit grain mass by defining $\tilde{n}(m,\, t)\,{\rm d}m$ as the number density of grains with mass between m and $m + {\rm d}m$; i.e. $\tilde{n}(m,\, t)\,{\rm d}m = n(a,\, t)\,{\rm d}a$. The grain mass is estimated as $m = \frac{4}{3}\pi a^3 s$ (i.e. grains are assumed to be spherical), where constant s is the material density of the grain. For the calculation of grain size distribution, we adopt $s = 3.3$ g cm^{-3} based on a silicate material. Using the fact that $\dot{a}$ is independent of a (Section 2.3), we obtain (see also Hirashita 2012)

$$\frac{\partial(m\tilde{n})}{\partial t} + \dot{m}\frac{\partial(m\tilde{n})}{\partial m} = \frac{1}{3}\dot{m}\tilde{n} + m\tilde{S}(m,\, t) + m\tilde{n}\frac{{\rm d}\ln\rho_{\rm gas}}{{\rm d}t}, \tag{3}$$

where $\dot{m} \equiv {\rm d}m/{\rm d}t = 4\pi a^2 s\dot{a}$ and $\tilde{S}(m,\, t)\,{\rm d}m = S(a,\, t)\,{\rm d}a$.

The dust-to-gas ratio as a function of time, $\mathcal{D}(t)$, is calculated by

$$\begin{aligned}\mathcal{D}(t) &= \frac{1}{\mu m_{\rm H} n_{\rm H}}\int_0^\infty \frac{4}{3}\pi a^3 s n(a,\, t)\,{\rm d}a \\ &= \frac{1}{\mu m_{\rm H} n_{\rm H}}\int_0^\infty m\tilde{n}(m,\, t)\,{\rm d}m.\end{aligned} \tag{4}$$

2.2 Supply from stars

2.2.1 Formulation

We consider the stellar population contributing to the dust supply in the local gas element considered above. Since we are interested in a system as old as the cosmic age, the current stellar population contributing to the dust formation is AGB stars, which originate from stars with $m < 8$ M$_\odot$ (m is the mass at the zero-age main sequence; e.g. Zhukovska et al. 2008). The dust mass density supplied from AGB stars per unit time, $\dot{\rho}_{\rm dust,AGB}$, is estimated as

$$\dot{\rho}_{\rm dust,AGB} = \int_{m_{t_{\rm age}}}^{m_{\rm up}} m_{\rm d}(m)\phi(m)\dot{\rho}_*(t_{\rm age} - \tau_m)\,{\rm d}m, \tag{5}$$

where $m_{t_{\rm age}}$ is the turn-off mass (i.e. the mass of the star whose lifetime is equal to the galaxy age $t_{\rm age}$), $m_{\rm up}$ is the upper cut-off of stellar mass, $m_{\rm d}(m)$ is the total dust mass produced by an AGB star with mass m, $\phi(m)$ is the stellar initial mass function (IMF), $\dot{\rho}_*(t_{\rm age})$ is the star formation rate density as a function of galaxy age, and τ_m is the lifetime of the star with mass m. We take the stellar lifetime from Raiteri, Villata & Navarro (1996). We adopt a Salpeter IMF [$\phi(m) \propto m^{-2.35}$] with $m_{\rm up} = 100$ M$_\odot$ and $m_{\rm low} = 0.1$ M$_\odot$, where $m_{\rm low}$ is the lower cut-off of stellar mass, and the normalization of the IMF is determined by $\int_{m_{\rm low}}^{m_{\rm up}} m\phi(m){\rm d}m = 1$. The data of dust yield $m_{\rm d}(m)$ is described in Section 2.2.2. We assume that dust grains ejected from AGB stars are instantaneously (on a time-scale shorter than 10^5 yr; Mathews & Brighenti 1999) injected into the hot gas (Temi et al. 2007). We approximate the star formation history with an instantaneous burst at $t_{\rm age} = 0$, which is a good approximation for nearby elliptical galaxies:

$$\dot{\rho}_*(t_{\rm age}) = \rho_{*,\rm tot}\delta(t_{\rm age}), \tag{6}$$

where $\rho_{*,\rm tot}$ is the total stellar mass density ever formed and $\delta(t)$ is Dirac's δ function. Noting that only stars with mass $m_{t_{\rm age}}$ are contributing to the current dust formation, we obtain from equations (5) and (6)

$$\dot{\rho}_{\rm dust,AGB} = m_{\rm d}(m_{t_{\rm age}})\phi(m_{t_{\rm age}})\rho_{*,\rm tot}\left|\frac{{\rm d}m_t}{{\rm d}t}\right|_{t=t_{\rm age}}. \tag{7}$$

Taking the mass loss of stars that have ended their lives into account, the current stellar mass, ρ_*, is estimated as

$$\rho_* = (1 - \mathcal{R})\rho_{*,\rm tot}, \tag{8}$$

where $\mathcal{R}$ is the returned fraction. We assume that $\mathcal{R} = 0.25$ (Kuo, Hirashita & Zafar 2013, this value is derived for $m_{t_{\rm age}} \simeq 1$ M$_\odot$, but is not sensitive to $t_{\rm age}$ as long as $t_{\rm age} > 10^9$ yr; Hirashita & Kuo 2011). Correspondingly, we adopt $t_{\rm age} = 9.5$ Gyr, the lifetime of $m = 1$ M$_\odot$ star. We fix $t_{\rm age}$, since we are interested in the time evolution at $t \lesssim 10^8$ yr, which is much shorter than $t_{\rm age}$.

Now, we formulate the source term in equation (1). This term expresses the dust input from AGB stars, and we hereafter refer to the dust supplied by AGB stars as *AGB dust*. We specify the grain size distribution of AGB dust in such a way that the source term in equation (1) is written as

$$S(a,\, t) = \dot{\rho}_{\rm dust} f_{\rm dust}(a), \tag{9}$$

where $f_{\rm dust}(a)$ is the grain size distribution function whose normalization is determined by

$$\int_0^\infty \frac{4}{3}\pi a^3 s f(a)\,{\rm d}a = 1. \tag{10}$$

Or equivalently, it is possible to use equation (3) with $\tilde{S}(m,\, t) = \dot{\rho}_{\rm dust}\tilde{f}_{\rm dust}(m)$, where the normalization of mass distribution function $\tilde{f}_{\rm dust}(m)$ is determined by $\int_0^\infty m\tilde{f}_{\rm dust}(m)\,{\rm d}m = 1$. For the grain size distribution, we consider two cases: one is a power-law form with the same power index as used in Tsai & Mathews (1995),

$$f_{\rm dust}(a) = C_{\rm M} a^{-3.5}\ (0.001\ \mu{\rm m} \le a \le 0.25\ \mu{\rm m}), \tag{11}$$

and the other is a lognormal form,

$$f_{\rm dust}(a) = \frac{C_l}{a}\exp\left\{-\frac{[\ln(a/a_0)]^2}{2\sigma^2}\right\}, \tag{12}$$

where $C_{\rm M}$ and C_l are the normalizing constants determined by equation (10), and a_0 and σ are the central grain radius and the standard deviation of the lognormal distribution, respectively. The first one (equation 11) is based on the one derived for the Milky Way ISM (Mathis, Rumpl & Nordsieck 1977), and is referred to as the MRN grain size distribution. The second one in equation (12) is based on the argument that AGB stars produce large (0.1–1 μm) grains (Asano et al. 2013b, and references therein). We adopt the same parameters as in Asano et al. (2013b): $a_0 = 0.1$ μm and $\sigma = 0.47$, which are based on theoretical calculations of dust condensation in AGB star winds by Yasuda & Kozasa (2012).

2.2.2 Dust yield of AGB stars

We take $m_{\rm d}(m)$ (the ejected dust mass by an AGB star for different progenitor mass) from theoretical calculations by Zhukovska et al. (2008), who adopted Ferrarotti & Gail (2006)'s framework to calculate the dust condensation in AGB star winds. Since we are interested in nearby elliptical galaxies, it is reasonable to consider the solar metallicity case ($Z = 0.02$). The stellar mass around 1 M$_\odot$, which is contributing to the current dust production, is relevant to this paper. Their calculations indicate that around 4×10^{-4}–10^{-3} M$_\odot$ of dust is produced by an $m = 1$–2 M$_\odot$ star. If we adopt $Z = 0.015$ (0.03) instead, the dust mass becomes three times as small (large) as the case above. Therefore, we should keep a factor of 3 uncertainty in mind. Ventura et al. (2014) also calculated theoretical dust yield for AGB stars, focusing on lower metallicities. Their highest metallicity case ($Z = 8 \times 10^{-3}$) shows that the dust mass produced by an AGB star with $m = 1$–$2\ \mathrm{M_\odot}$ is 2×10^{-4}–10^{-3} $\mathrm{M_\odot}$, similar to that adopted above.

2.3 Sputtering

The changing rate of grain radius by sputtering, $\dot{a}$, in equation (1) is estimated by a fitting formula derived by Tsai & Mathews (1995):

$$\dot{a} = -\tilde{h}\left(\frac{\rho_{\rm gas}}{m_{\rm H}}\right)\left[1+\left(\frac{\tilde{T}}{T}\right)^{2.5}\right]^{-1}, \tag{13}$$

where the coefficients of this fitting function, $\tilde{h} = 3.2 \times 10^{-18}\ \mathrm{cm^4\ s^{-1}}$ and $\tilde{T} = 2 \times 10^6$ K, are determined to give a good fit to the sputtering rate of both silicate and graphite in Draine & Salpeter (1979). This formula correctly reproduces the temperature dependence of sputtering in that it is efficient at $T \gtrsim 2 \times 10^6$ K and steeply declines at $T \lesssim 10^6$ K (Nozawa et al. 2006). We also define the sputtering time-scale, $\tau_{\rm sput} \equiv |a/\dot{a}|$, which is estimated at $T \gtrsim \tilde{T}$ using equation (2) as

$$\tau_{\rm sput} \simeq \frac{a}{\tilde{h}\mu n_{\rm H}} \simeq 7.1 \times 10^5 \left(\frac{a}{1\ \mu\mathrm{m}}\right)\left(\frac{n_{\rm H}}{1\ \mathrm{cm^{-3}}}\right)^{-1}\ \mathrm{yr}. \tag{14}$$

This is consistent with the values derived by a detailed treatment of sputtering yield (Nozawa et al. 2006, see their fig. 2).

2.4 Cooling of the hot ISM

Following Mathews & Brighenti (2003), we assume that the gas pressure in the local region of interest is constant. The time evolution of the gas temperature T through isobaric cooling is described by (Mathews & Brighenti 2003)

$$\frac{\mathrm{d}T}{\mathrm{d}t} = -\frac{2\Lambda_{\rm tot}(T)}{5nk}, \tag{15}$$

where $\Lambda_{\rm tot}(T)$ is the cooling rate (energy lost per volume per time) including both gas and dust cooling, n is the number density of gas particles, and k is the Boltzmann constant. Assuming that H and He are fully ionized, we estimate that $n = 2.3n_{\rm H}$.

The cooling rate by gas emission is taken from Sutherland & Dopita (1993). Specifically, we adopt $n_{\rm t}n_{\rm e}\Lambda_{\rm N}(T)$ [$\Lambda_{\rm N}(T)$ is the cooling function for gas cooling] for the cooling rate per volume with electron number density $n_{\rm e} = 1.2n_{\rm H}$ and total number density of ions $n_{\rm t} = 1.1n_{\rm H}$. We stop the calculation when T reaches 10^5 K (this time is denoted as t_5), below which the temperature evolution occurs much faster and the effect of recombination would change $n_{\rm e}$ significantly. Since sputtering does not work at such a low temperature, the resulting grain abundance and size distribution are insensitive to the detailed treatment of thermal evolution at $\lesssim 10^5$ K.

The gas also cools through gas–grain collisions (e.g. Dalgarno & McCray 1972; Dwek 1987; Seok, Koo & Hirashita 2015). The rate of this dust cooling is estimated as $n_e n_{\rm H}\Lambda_{\rm d}(T)$, where $\Lambda_{\rm d}(T)$ is the cooling function for dust cooling. We compute $\Lambda_{\rm d}(T)$ based on Dwek (1987) under the dust abundance and grain size distribution calculated in this paper. We again adopt $n_e = 1.2n_{\rm H}$ and assume silicate as dust species (adopting graphite instead does not significantly change the cooling rate; Dwek 1987).

After all, we evaluate the total cooling rate as $\Lambda_{\rm tot} = n_{\rm t}n_e\Lambda_{\rm N} + n_e n_{\rm H}\Lambda_{\rm d}$. We assume a constant pressure, so that the density is simultaneously varied as

$$\frac{\mathrm{d}\ln\rho_{\rm gas}}{\mathrm{d}t} = -\frac{\mathrm{d}\ln T}{\mathrm{d}t}. \tag{16}$$

Table 1. Model parameters adopted from Tsai & Mathews (1995).

Model	L_B ($10^{10}\ \mathrm{L_\odot}$)	ρ_* ($\mathrm{g\ cm^{-3}}$)	$\rho_{\rm gas}$ [a] ($\mathrm{g\ cm^{-3}}$)	T (10^7 K)
a	10.6	1.19×10^{-21}	1.43×10^{-25}	0.922
b	3.31	1.36×10^{-20}	3.01×10^{-25}	0.468
c	0.976	1.83×10^{-19}	8.74×10^{-25}	0.252

Notes. The densities at the core radius are adopted.
[a]The corresponding hydrogen number densities are $n_{\rm H} = 0.0610$, 0.128, and 0.373 $\mathrm{cm^{-3}}$ for Models a, b, and c, respectively.

2.5 Models and ICs

For simplicity, we only focus on a 'typical' single region in an elliptical galaxy by adopting representative gas density and temperature. Tsai & Mathews (1995) considered three models of elliptical galaxies which are classified by B-band luminosities, L_B. The models are referred to as Models a, b, and c depending on the B-band luminosity. Although we do not directly use B-band luminosity, the quantities used in the models (ρ_*, $\rho_{\rm gas}$, T) are related to it. In Table 1, we list the adopted parameters for each model. The values at the core radius are adopted for the star and gas densities. (We convert the central densities given in table 1 of Tsai & Mathews 1995 to the values at the core radius by assuming the radial profiles given in that paper.) The stellar mass density ρ_* is used to estimate the dust supply rate from AGB stars (Section 2.2.1), and the gas density $\rho_{\rm gas}$ and gas temperature T are used for the initial conditions (ICs).

We start with no dust ($\mathcal{D}_0 = 0$, where $\mathcal{D}_0$ is the initial dust-to-gas ratio), referred to as *the dust-free IC*, or $\mathcal{D}_0 = 0.0075$, referred to as *the dusty IC*. The latter value of $\mathcal{D}_0$ is typical of the solar-metallicity ISM and the same functional form for the grain size distribution as equation (11) [i.e. $n(a, t = 0) \propto a^{-3.5}$] is assumed with the normalization determined by equation (4). We expect that the realistic situation lies between these two extreme conditions for the IC, but that the dust-free IC is more realistic considering that the dust is rapidly destroyed by sputtering as shown below. Thus, we focus on the dust-free IC as a 'fiducial' model. As we explained above, we investigate two cases for the grain size distribution of AGB dust: MRN and lognormal.

3 RESULTS

3.1 Thermal evolution and dust-to-gas ratio

The thermal evolution of the hot gas is of fundamental importance in determining the fate of dust. On the other hand, the temperature of hot gas could also be affected by dust cooling. For dust cooling, the dust abundance is the key factor. Thus, we first show the time evolutions of gas temperature (T) and dust-to-gas ratio ($\mathcal{D}$) in Figs 1 and 2, respectively.

We compare the results with the different two ICs for the dust-to-gas ratio, $\mathcal{D}_0 = 0$ and 0.0075 (dust-free and dusty ICs, respectively). We adopt the MRN grain size distribution for AGB dust. As shown in Fig. 1, the temperature drops more rapidly for the dusty IC than for the dust-free IC because of more efficient dust cooling. The time at which the temperature drops down to 10^5 K, t_5, is by a factor of $\sim$1.5 shorter for the dusty IC than for the dust-free IC. In Table 2,

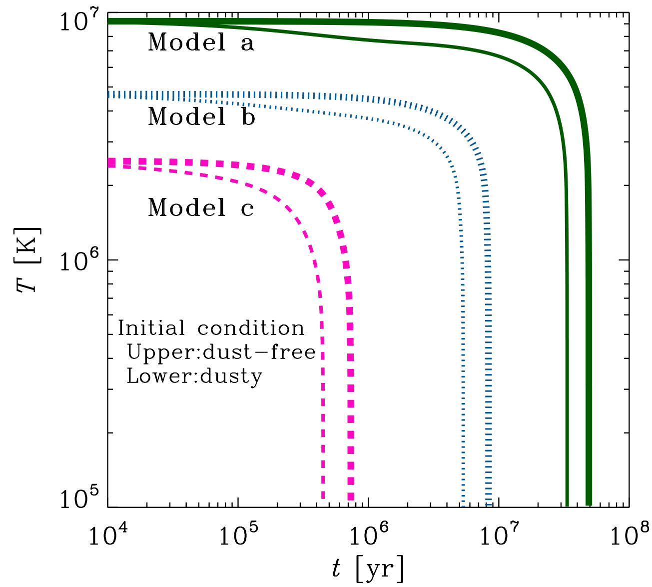

Figure 1. Time evolution of gas temperature T. Note that the gas density is always inversely proportional to T during the entire evolution. The upper thicker (lower thinner) solid, dotted, and dashed lines present the results for Models a, b, and c, respectively, with the dust-free IC, $\mathcal{D}_0 = 0$ (with the dusty IC, $\mathcal{D}_0 = 0.0075$). The MRN grain size distribution is adopted for AGB dust. The evolutionary tracks of the cases without cooling and with the lognormal size distribution of AGB dust for $\mathcal{D}_0$ both overlap with the thick lines (thus, they are not shown in the figure), which means that dust cooling does not affect the thermal evolution of the hot gas for the dust-free IC.

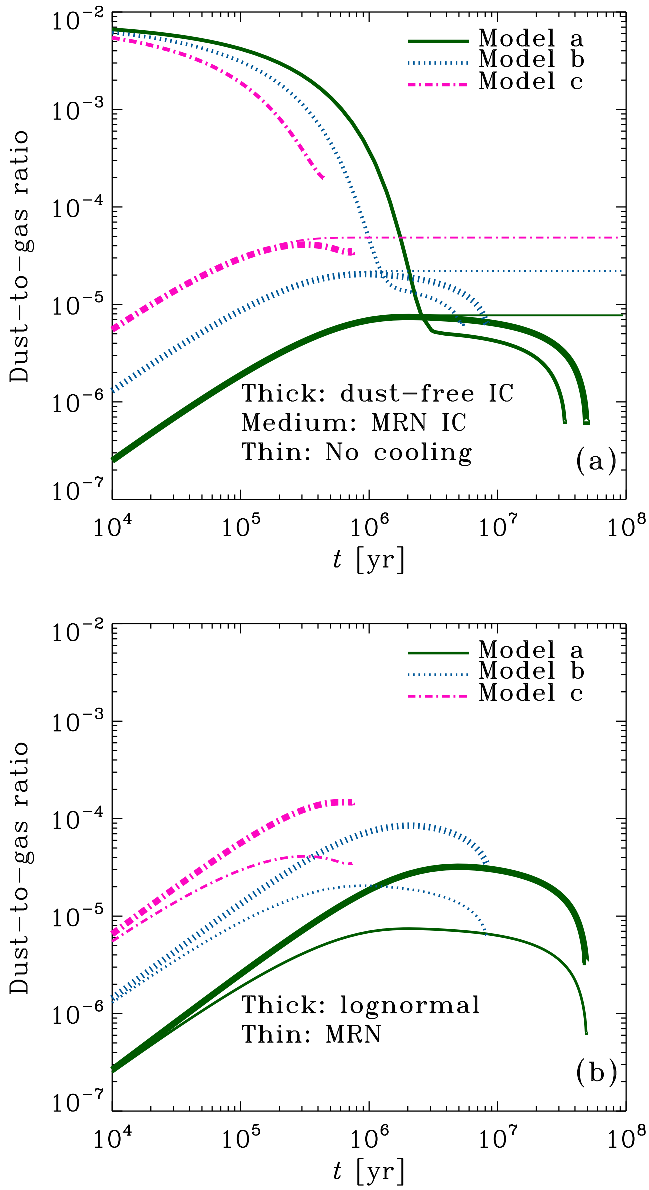

Figure 2. Time evolution of dust-to-gas ratio $\mathcal{D}$. (a) The MRN grain size distribution is adopted for AGB dust. The solid, dotted, and dashed lines present the results for Models a, b, and c, respectively, with the dust-free and dust-rich ICs (lines with enhanced and medium thickness, respectively) with cooling included, and with the dust-free IC without cooling (thin lines). In the cases with cooling, the calculation is stopped when the gas temperature reaches 10^5 K (i.e. at time t_5). (b) Comparison between the two different grain size distributions of AGB dust: lognormal (thick lines) and MRN (thin lines). The solid, dotted, and dashed lines present the results for Models a, b, and c, respectively.

we list t_5 for each galaxy model with different $\mathcal{D}_0$ and grain size distributions of AGB dust.

In Fig. 2, we show the evolution of dust-to-gas ratio, $\mathcal{D}$, calculated by equation (4). First we explain the evolution of $\mathcal{D}$ for the dust-free IC. At the beginning of the evolution, the dust-to-gas ratio increases because of the dust supplied from the AGB stars. The increase of $\mathcal{D}$ is saturated because of the destruction by sputtering. At this stage, the dust-to-gas ratio approaches to the value determined by the balance between dust supply and destruction as we show later. Indeed, the sputtering time-scale given by equation (14) (note that $a < 0.25$ µm for the MRN grain size distribution) is much shorter than t_5, which allows the grain size distribution to approach the equilibrium between supply and destruction. At the end, the dust-to-gas ratio decreases because the compression of the gas due to the temperature drop by cooling enhances the sputtering rate (but the temperature is still higher than $\sim 2 \times 10^6$ K). Indeed, the decrease of dust-to-gas ratio coincides with the temperature drop (Fig. 1). As shown in equation (13), the sputtering efficiency scales as $\propto \rho_{\rm gas}$ at any gas temperature, while it is not sensitive to the gas temperature as long as $T \gtrsim \tilde{T} = 2 \times 10^6$ K. Because the effect of density is larger than that of temperature, cooling eventually enhances the dust destruction, contrary to the expectation by Mathews & Brighenti (2003).

In order to show the level of $\mathcal{D}$ achieved by the equilibrium between dust supply and destruction under the initial gas density, we also show the cases where we neglect cooling (i.e. the gas temperature and density are constant) in Fig. 2. In these cases without cooling, the dust-to-gas ratio is the same as the above case at the beginning of evolution before the gas cools significantly, and it approaches to the value determined by the balance between dust supply and sputtering. The dust-to-gas ratio achieved by the equilibrium is the highest in Model c, primarily because of the highest stellar mass per gas mass (i.e. the highest dust supply rate per gas mass).

We also present the results for the dust-rich ICs ($\mathcal{D}_0 = 0.0075$) in Fig. 2a. In Models a and b, the final dust-to-gas ratio at t_5 is almost the same regardless of $\mathcal{D}_0$ (note that t_5 is different, though, between the different ICs; Table 2). On the other hand, the effect of IC on the final dust-to-gas ratio remains in Model c, because the evolution starts with lower temperature so the effect of sputtering is smaller

Table 2. Time (t_5) at which the temperature drops down to 10^5 K.

IC[a]	AGB dust[b]	Model a t_5 (yr)	Model b t_5 (yr)	Model c t_5 (yr)
Dust-free	MRN	4.9×10^7	8.3×10^6	7.3×10^5
Dusty	MRN	3.3×10^7	5.3×10^6	4.5×10^5
Dust-free	lognormal	4.9×10^7	8.3×10^6	7.4×10^5
Dust-free	no dust[c]	5.0×10^7	8.6×10^6	7.4×10^5

Notes. [a]The IC is chosen from the dust-free and the dusty cases with the initial dust-to-gas ratio $\mathcal{D} = 0$ and 0.0075, respectively. For the dusty initial condition, the grain size distribution is assumed be the MRN (i.e. power law with an index of −3.5; see the text for details).
[b]The grain size distribution of AGB dust is chosen from MRN or lognormal.
[c]This case is for no dust cooling (i.e. only gas cooling).

than Models a and b. Yet, even in the dusty IC of Model c, the dust-to-gas ratio at $t = t_5$ is much lower than the initial dust-to-gas ratio ($\mathcal{D}_0 = 0.0075$).

Although the large fraction of the initial dust is destroyed in any case, the IC has an imprint on the temperature evolution as shown in Fig. 1. Therefore, if the initial dust-to-gas ratio is as large as the value in the Milky Way ISM, dust cooling has a significant influence on the thermal evolution of the gas. However, such a high dust-to-gas ratio is never achieved if the dust enrichment and destruction take place simultaneously.

In order to show the effect of AGB dust, we also examine the cases with and without dust enrichment for the dust-free IC, finding that dust cooling by AGB dust has little influence on the thermal evolution of the hot ISM. Indeed, the evolutionary track is indistinguishable between the cases with and without dust enrichment (thus, the case without dust enrichment is not shown in Fig. 1). This is also clear from Table 2 (compare the first and last rows): t_5 is only slightly longer with no dust cooling than with dust cooling. We also confirmed that change of the grain size distribution of AGB dust to the lognormal size distribution does not alter the thermal history. Indeed as shown in Table 2, t_5 is almost identical between the MRN and lognormal AGB dust.

In Fig. 2b, we examine the effects of the grain size distribution of AGB dust on the evolution of $\mathcal{D}$. Since the lognormal grain size distribution is more biased to large sizes than the MRN grain size distribution, it has a longer sputtering time-scale $\tau_{\rm sput}$ (equation 14). The final dust-to-gas ratio at $t \sim t_5$ in the lognormal case is about four times as large as in the MRN case. Nevertheless, since the dust abundance is still kept much lower than 0.01 by dust destruction, the temperature evolution is not affected by dust cooling even in the lognormal case as mentioned above.

3.2 Grain size distribution

Now we examine the evolution of grain size distribution in detail. In Fig. 3, we show the evolution of grain size distribution for the dust-free IC. The MRN grain size distribution is adopted for AGB dust. In the initial stage at $t \ll t_5$, when the change of gas density due to cooling is negligible, the grain abundance gradually increases, converging to the equilibrium grain size distribution determined by the balance between the supply from AGB stars and the destruction by sputtering, and the slope is described by $n(a) \propto a^{-2.5}$ (Appendix B). We have already seen above that the dust-to-gas ratio approaches to the equilibrium value. As is also observed above in Fig. 2, the grain abundance decreases at the final stage of evolution around $t \sim t_5$ because the density increase by cooling enhances the sputtering rate.

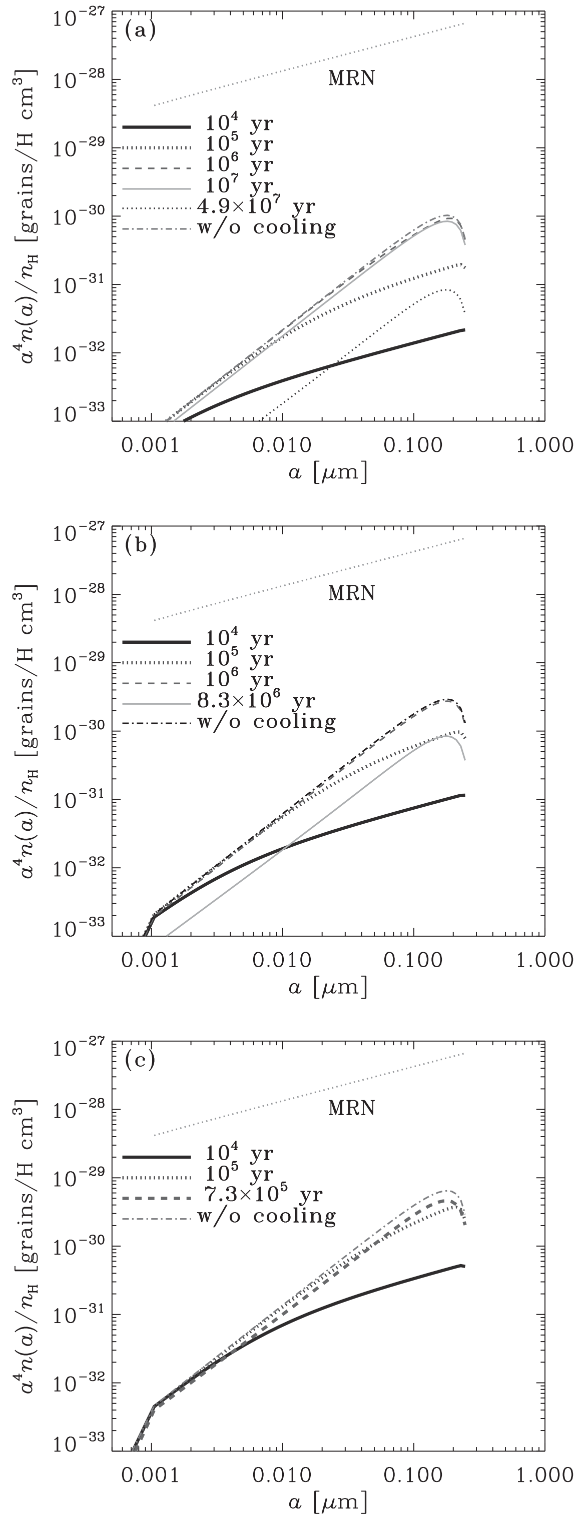

Figure 3. Grain size distribution per hydrogen atom for different times. The dust-free IC is adopted. Grain size distributions are multiplied by a^4 to show the grain mass distribution per logarithmic grain radius. Panels (a), (b), and (c) show the results for Models a, b, and c, respectively. The correspondence of the line species to the time is shown in each panel. The dotted line marked as 'MRN' is the MRN grain size distribution with a dust-to-gas ratio of 0.0075, shown as a reference for the grain size distribution appropriate for the Milky Way ISM. Note that the final time (t_5) in each model is determined by the time when the gas temperature reaches $T = 10^5$ K. The dot–dashed line shows the equilibrium grain size distribution without dust cooling.

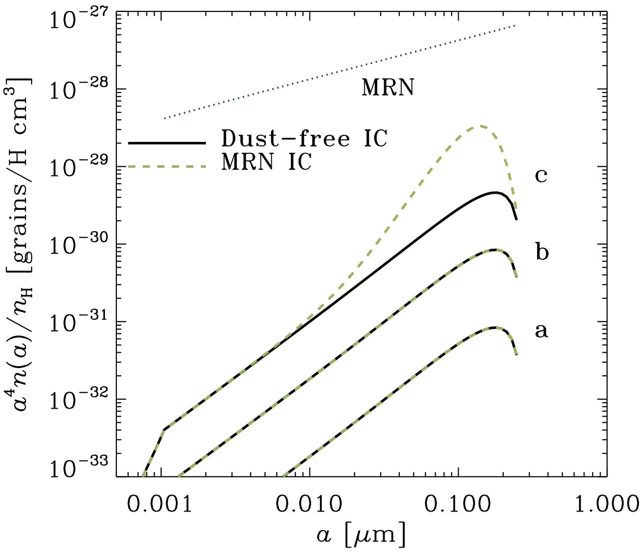

Figure 4. Grain size distributions at $t = t_5$ (after cooling) per hydrogen atom (multiplied by a^4). Solid and dashed lines show the results for the dust-free ($\mathcal{D}_0 = 0$) and dust-rich ($\mathcal{D}_0 = 0.0075$) ICs (IC), respectively. The dotted line marked as 'MRN' is the MRN grain size distribution with a dust-to-gas ratio of 0.0075, shown as a reference for the grain size distribution appropriate for the Milky Way ISM.

This is the reason why the grain size distributions shift downwards at the final stage in all the three models.

In Fig. 4, we compare the grain size distributions at $t = t_5$ for the three models with the dust-free and dust-rich ICs (the MRN grain size distribution is adopted for AGB dust). As is consistent with Fig. 2, the dust abundance per hydrogen atom (or the dust-to-gas ratio) is the largest in Model c: as explained above, this is due to the highest stellar mass per gas mass (Table 1), that is, the highest dust supply rate per gas mass. Moreover, the comparison between the cases of different $\mathcal{D}_0$ in Models a and b shows almost no difference, which indicates that almost all the dust that existed initially in the hot gas has been destroyed. In Model c, the effect of IC remains as explained in Section 3.1 (Fig. 2): this is because of the low temperature, i.e. low sputtering rate. The difference in the IC affects at the largest grain sizes because the largest grains have the longest sputtering time-scale (equation 14). However, even in Model c, the grain abundance decreases far below the initial MRN size distribution (shown by the dotted line in Fig. 4). Therefore, in all cases, the final grain size distribution deviates significantly from the initial grain size distribution.

We also examine the case of the lognormal size distribution for AGB dust (equation 12). We adopt the dust-free IC. The resulting grain size distributions are shown in Fig. 5, and their evolutionary behaviour is similar to the case of the MRN grain size distribution in the following aspects: the grain abundance increases before significant cooling occurs (i.e. at $t \ll t_5$), converging to the equilibrium grain size distribution (Appendix B), while it decreases after cooling (i.e. around $t \sim t_5$). Compared with the lognormal function, the tail towards small grain sizes becomes prominent in the final grain size distributions at $t = t_5$. This tail is due to the continuous destruction of large grains by sputtering and described by $n(a) =$ constant (Appendix B). The grain abundance is reduced around $t = t_5$ because the increase of gas density by cooling enhances the sputtering rate, as explained above.

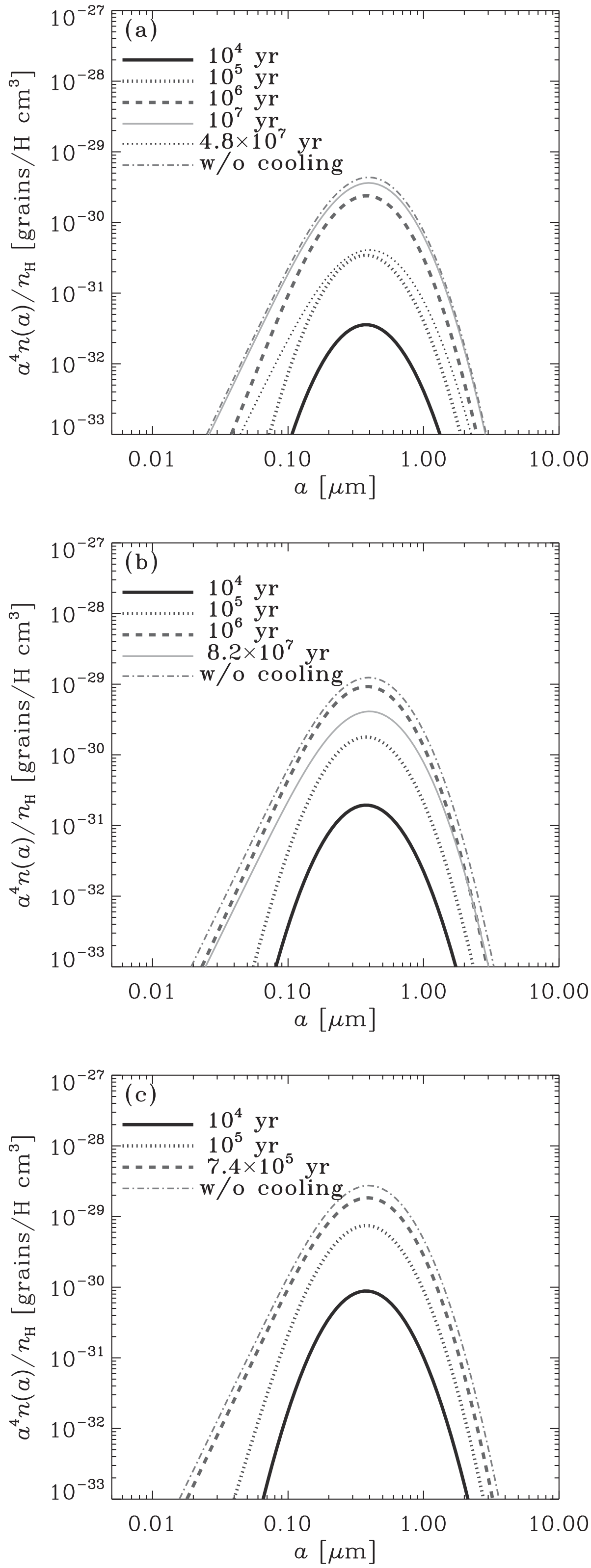

Figure 5. Same as Fig. 3 but for the lognormal size distribution of AGB dust. Panels (a), (b), and (c) show the results for Models a, b, and c, respectively. The correspondence of the line species to the time is shown in each panel. Note that the final time (t_5) in each model is determined by the time when the gas temperature reaches $T = 10^5$ K. The dot–dashed line shows the equilibrium grain size distribution without dust cooling.

4 PROCESSING AFTER COOLING

In the above, we have traced the dust evolution in the hot gas up to the point where the gas cools down to 10^5 K. After that, sputtering does not act as a dust processing mechanism any more, but the dust may still be processed by other mechanisms than sputtering. In particular, many authors have argued the importance of dust growth by the accretion of gas-phase metals for the total dust budget in star-forming galaxies (e.g. Dwek 1998). Since this accretion mechanism works in cold and dense clouds, it is worth investigating a possibility of dust growth also in the cold gas in elliptical galaxies. As mentioned in the Introduction (and shown in Section 3), it has been argued that the observed dust abundance in elliptical galaxies cannot be explained by the internal dust supply from AGB stars because of rapid destruction by sputtering. Thus, we examine dust growth as a potential additional source of dust in elliptical galaxies (see also Fabian et al. 1994; Voit & Donahue 1995; Martini, Dicken & Storchi-Bergmann 2013).

Under a high pressure in the inner part of elliptical galaxy, a cold phase with $T \sim 10^2$ K is preferred rather than a warm phase with $T \sim 10^4$ K (Wolfire et al. 1995). Such a cold dense medium is indeed suitable for the site of dust growth. Since accretion and coagulation (grain–grain sticking) both occur in such a cold dense medium, we treat them simultaneously (Hirashita 2012); however, as shown later, coagulation only plays a minor role. Below we calculate the dust evolution driven by accretion and coagulation in the cold gas, starting from the grain size distributions achieved after cooling of the hot gas.

4.1 Formulation of accretion and coagulation

We calculate the evolution of grain size distribution by accretion and coagulation using the formulation in Hirashita (2012), which has a wide application to, for example, polarization predictions (Voshchinnikov & Hirashita 2014). Again, the silicate dust properties are assumed, but adopting carbonaceous dust instead does not change the evolution of grain size distribution significantly (Hirashita 2012). If we consider the pressure equilibrium with the hot gas, $n_{\rm H} > 10^3$ cm^{-3} is achieved for all models at a temperature appropriate for the cold ISM ($T \sim 10^2$ K). Thus, we conservatively assume that $n_{\rm H} = 10^3$ cm^{-3}, but the results for other densities can be easily obtained by noting that the time-scale of grain processing is simply proportional to $n_{\rm H}^{-1}$. The gas temperature, which determines the thermal speed of the accreting material is assume to be 10^2 K. The available gas-phase metals (in our case, silicon) is estimated based on the solar abundance of Si, (Si/H) = 3.55×10^{-5} (Däppen 2000). We also assume that the mass fraction of Si in silicate is 0.166. The grain velocity, used to estimate the grain–grain collision rate for coagulation, is treated as a function of grain radius, and is taken from the molecular cloud case in Yan, Lazarian & Draine (2004), which has a similar gas density to the one considered here. We also impose the same coagulation threshold velocity as adopted in Hirashita & Yan (2009, originally based on Chokshi, Tielens & Hollenbach 1993; Dominik & Tielens 1997): only if the relative velocity is below this threshold, which varies with the sizes of colliding grains, the grains coagulate. However, detailed treatment of coagulation does not affect the results, because, as shown later, the abundant gas-phase metals make the role of accretion stronger than that of coagulation in changing the grain size distribution. For the IC of each model, we use the grain size distribution achieved in the hot gas after cooling. More specifically, the initial grain size distribution is produced by multiplying the grain size distributions per hydrogen at $t = t_5$, $n(a, t_5)/n_{\rm H}$, in Section 3 by $n_{\rm H} = 10^3$ cm^{-3}. The time is newly measured from the onset of grain growth in the cold gas; to avoid the confusion, we use a different notation for the time, t', measured from the onset of grain growth.

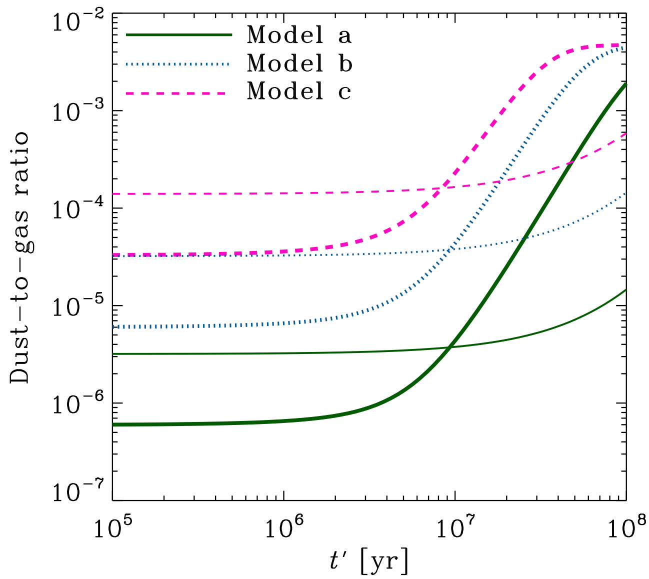

Figure 6. Time evolution of dust-to-gas ratio $\mathcal{D}$ by dust growth. The time t' is the elapsed time from the onset of dust growth in cooled gas. The thick solid, dotted, and dashed lines present the results for Models a, b, and c in the case where we use the result of the MRN AGB dust calculation at t_5 for the IC (i.e. the final state of each model in Fig. 3 is used for the IC). The thin lines with the same line species represent the results for the lognormal AGB dust calculation at t_5 (i.e. the final state of each model in Fig. 5 is used for the IC).

4.2 Results

First, we show in Fig. 6 the evolution of dust-to-gas ratio $\mathcal{D}$ estimated by equation (4) at $t' \le 10^8$ yr (as shown later, the observed extinction curves are well covered by the grain size distributions at $t' \le 10^8$ yr). Note that accretion changes $\mathcal{D}$ while coagulation does not. If we start with the grain size distribution at t_5 for the MRN AGB dust, $\mathcal{D}$ begins to increase drastically from $t' \sim$ afew $\times$ 10^6 yr and reaches 10^{-3} in a few $\times$ 10^7 yr. Therefore, if the lifetime of the cold gas is longer than 10^7 yr, there is a possibility of dust 'reformation' using the remnants of sputtered dust grains, which explains the observed level of dust abundance as we discuss in the next section. The increase of $\mathcal{D}$ saturates most quickly in Model c simply because the initial dust abundance is the largest, which also means that the abundance of available gas-phase metals is the lowest.

For the calculation adopting the lognormal AGB dust case for the IC, as shown in Fig. 6, the increase of dust-to-gas ratio is not so drastic as in the case of MRN AGB dust models because the grain size distribution is biased to large sizes (the accretion time-scale is proportional to the grain radius; Hirashita 2012). This indicates that the initial grain size distribution in the cold gas, which is the final grain size distribution of the cooled hot gas, is of fundamental importance in determining the efficiency of dust mass increase in the cold gas.

Next, we investigate the evolution of grain size distribution by accretion and coagulation. In Fig. 7, we show the evolution of grain size distribution, adopting the MRN AGB dust case for the IC. We

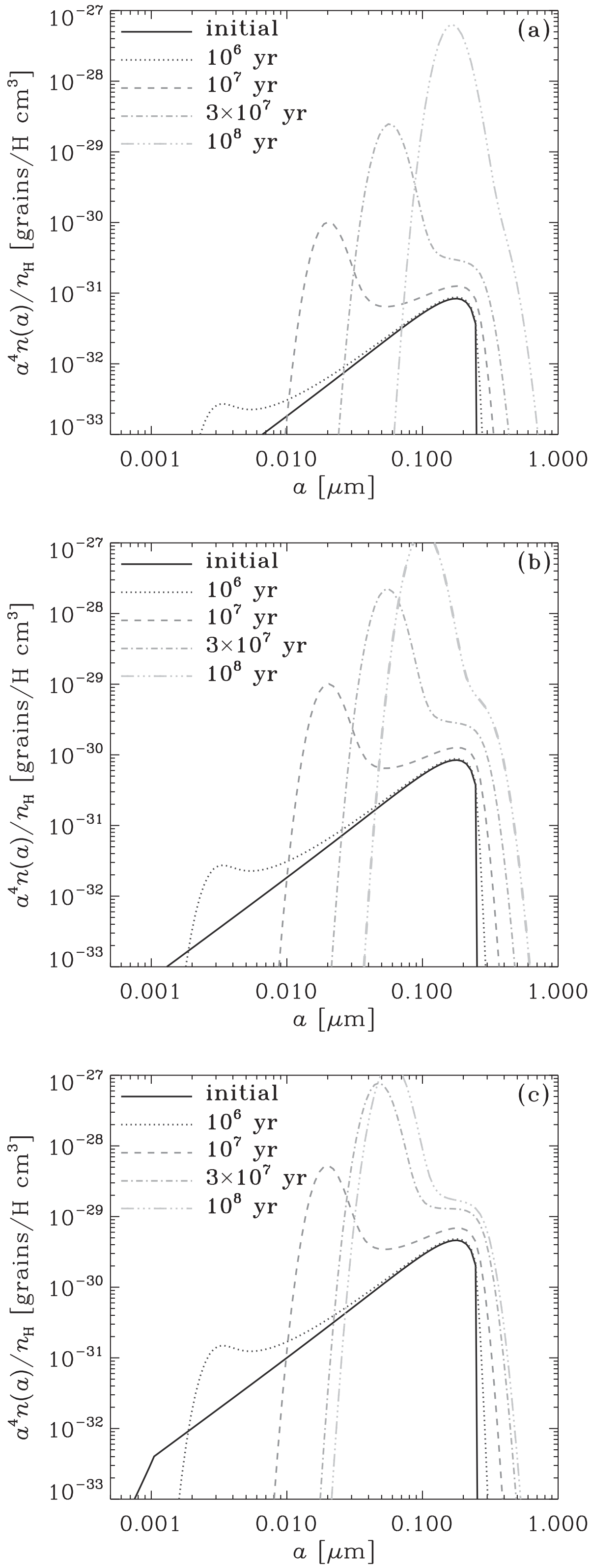

Figure 7. Evolution of grain size distribution by grain growth, starting from the final grain size distributions in Fig. 3. Panels (a), (b), and (c) show the results for Models a, b, and c, respectively. The solid, dotted, dashed, dot–dashed, triple-dot–dashed lines present the grain size distributions at $t' = 0$, 10^6, 10^7, 3×10^7, and 10^8 yr, respectively. We assume $n_\mathrm{H} = 10^3$ cm^{-3}, but the time-scale just scales as $\propto n_\mathrm{H}^{-1}$.

observe that accretion continue to increase the dust abundance over $\sim 10^8$ yr, which is consistent with the evolution of $\mathcal{D}$ shown above. Because accretion saturates most quickly in Model c as explained above, the grain radii achieved by the growth are the smallest in Model c.

The most important feature of grain growth by accretion is that the effect appears most significantly at the smallest grain sizes. As explained in Hirashita (2012), accretion enhances the dust abundance at the smallest grain sizes, which have the shortest accretion time-scale because of the largest grain surface-to-volume ratio. In order to isolate the effect of accretion, we also examined the grain size distribution with only accretion (i.e. without coagulation). We confirmed that there is almost no difference between the cases with and without coagulation (we do not plot the results because the grain size distributions with and without coagulation are almost indistinguishable). This is partly because the effect of accretion is enhanced by the large amount of available gas-phase metals, partly because coagulation does not proceed beyond $a \sim 0.1$ µm at which grains have larger velocities than the coagulation threshold (this means that the creation of larger grains than $\sim$0.1 µm only occurs by accretion).

In Fig. 8, we show the same plot as above but we adopt the lognormal AGB dust case (i.e. the final grain size distribution in each panel of Fig. 5) for the IC. We observe that the change of the grain size distribution occurs more slowly than the MRN AGB dust case because the grains are biased to larger sizes (recall that the accretion time-scale is proportional to the grain radius). Therefore, grain growth is very sensitive to the size distribution of the grains incorporated in the cold medium. However, as shown later, extinction curves calculated for the lognormal AGB dust cases are too flat and are inconsistent with the observed extinction curves (Section 5.2).

5 OBSERVATIONAL PROPERTIES AND DISCUSSION

5.1 Dust abundance

For comparison of dust abundance, we adopt elliptical galaxy samples observed by *Herschel* from Smith et al. (2012) and di Serego Alighieri et al. (2013). The dust-to-gas ratio is estimated for each galaxy based on the dust mass derived from the *Herschel* FIR emission and the gas mass estimated by the sum of H I and H_2 masses (the latter is from CO luminosity). The sample galaxies adopted are listed in Table 3. For the sample in Smith et al. (2012), we select four galaxies with (i) a morphological type of elliptical galaxies (E); (ii) detection of FIR emission (i.e. a successful estimate of dust mass); and (iii) detection of H I mass. We use the upper limits for H_2 mass, but the treatment of H_2 mass does not affect the results since these upper limits of H_2 mass are significantly smaller than the H I mass. For the sample in di Serego Alighieri et al. (2013), we exclude galaxies with morphological type of S0 and Sa and only select the objects for which both H I and H_2 masses are constrained (i.e. detected or with an upper limit obtained). As a consequence, we adopt four objects from their sample. NGC 4374 is common to both samples. The *B*-band and X-ray luminosities are taken from O'Sullivan et al. (2001).

As seen in Table 3, the observed dust-to-gas ratio is larger than 10^{-4}. However, as shown in Fig. 2, this level of dust-to-gas ratio cannot be achieved in the hot ISM, especially in Models a and b, which are appropriate for most of the *B*-band luminosities of the sample. The situation does not change even if we change the grain size distribution of AGB dust to the lognormal distribution

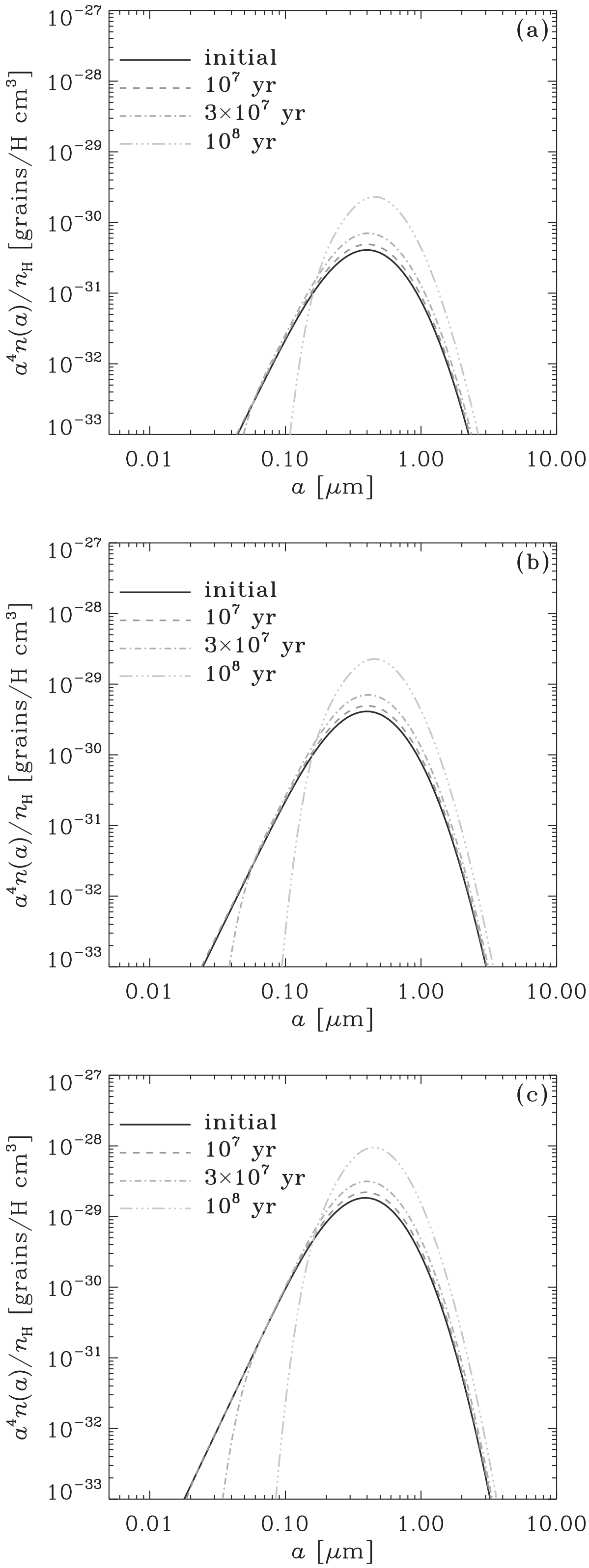

Figure 8. Evolution of grain size distribution by grain growth, starting from the final grain size distributions in Fig. 5. Panels (a), (b), and (c) show the results for Models a, b, and c, respectively. The solid, dashed, dot–dashed, triple-dot–dashed lines present the grain size distributions at $t' = 0$, 10^7, 3×10^7, and 10^8 yr, respectively. We assume $n_{\rm H} = 10^3$ cm^{-3}, but the time-scale just scales as $\propto n_{\rm H}^{-1}$.

(Fig. 2b). This confirms previous conclusions derived by various authors that the dust destruction in the hot gas phase prevents the dust-to-gas ratio (or the total dust mass) from reaching the observed level (Goudfrooij & de Jong 1995; Patil et al. 2007), and shows that this is also true even if we consider the grain size distribution. We have also shown that cooling does not help the dust to survive, contrary to Mathews & Brighenti (2003)'s expectation: gas compression caused by cooling enhances the sputtering efficiency, leading to an additional decrease of the dust abundance. In other words, the effect of cooling further emphasizes the discrepancy between the expected and observed dust abundances in elliptical galaxies.

Some authors argue an external origin of the gas and dust based on the evidence that the kinematic properties of the gas are decoupled from those of the major stellar component in some elliptical galaxies (Forbes 1991; Caon, Macchetto & Pastoriza 2000). Since not all the galaxies fit this external-origin scenario (Forbes 1991), it is still worth considering how much dust could be explained by the 'internal-origin' scenario in which the dust is produced by their own stellar populations and/or inherent dust growth mechanisms.

Regarding the internal origin of dust, we have shown that the accretion of gas-phase metals in cold clouds increases the dust-to-gas ratio to a level of $\sim 10^{-3}$ in $\sim 10^7$–10^8 yr. In this sense, cooling is important in the dust abundance, not through survival in the hot gas (as in Mathews & Brighenti 2003's original idea) but through the formation of cold clouds hosting dust growth. The time-scale of the dust abundance increase by dust growth is shorter than the feedback time-scale ($\gtrsim 10^8$ yr; Kaviraj et al. 2011; Pellegrini, Ciotti & Ostriker 2012), on which AGN activity heats the cooled gas. Therefore, the 'recovery' of dust by accretion is a plausible scenario of explaining the observed excessive dust abundance in elliptical galaxies.

5.2 Extinction curves

The grain size distributions obtained by our calculations are tested against the observed extinction curves in Patil et al. (2007). Based on the calculated grain size distributions above, we theoretically predict the corresponding extinction curves. The extinction at wavelength λ in units of magnitude (A_λ) is calculated by weighting the extinction efficiency factor $Q_{\rm ext}(a, \lambda)$ with the grain size distribution $n(a)$ as

$$A_\lambda = C \int_0^\infty n(a)\pi\, a^2 Q_{\rm ext}(a,\ \lambda){\rm d}a, \tag{17}$$

where C is the normalizing constant, which cancels out when we consider the ratio of A_λ at two wavelengths later. Although we assumed silicate for the grain property, the grain growth time-scale of carbonaceous dust is similar (Hirashita 2012). The steepness of extinction curve is often discussed in comparison with the Milky Way extinction curve. Therefore, we simply assume a mass fraction of 0.54:0.46 for silicate and carbonaceous dust (graphite), which fits the Milky Way extinction curve under the MRN grain size distribution (Hirashita & Yan 2009). We refer to Hirashita & Yan (2009) for the adopted parameters for silicate and graphite. However, since we are interested in wavelengths longer than 0.4 μm, the extinction curve slope is broadly determined by the grain size distribution with a minor effect of the material.

Now we examine the extinction curves in the MRN AGB dust case. In Fig. 9, we show the extinction curves for the grain size distributions at t_5 in Fig. 3 (i.e. the initial grain size distributions before grain growth) and the variation of extinction curves by grain

Table 3. Elliptical galaxy sample adopted from Smith et al. (2012) and di Serego Alighieri et al. (2013).

Name	Other name	$\log L_B$ ($L_\odot$)	$\log L_X$ (erg s^{-1})	$\log M_{dust}$ ($M_\odot$)	$\log M_{HI}$ ($M_\odot$)	$\log M_{H_2}$ ($M_\odot$)	$\log \mathcal{D}$	Ref.[a]
VCC 763	NGC 4374, M84	10.57	40.83	5.05[b]	8.96	<7.23	− 3.91[c]	1, 2, 3
HRS 150	NGC 4406, M86	10.66	42.05	6.63	7.95	<7.4	− 1.43[c]	1, 3
HRS 186	NGC 4494	10.62	<40.10	5.08	8.26	<7.35	− 3.23[c]	1, 3
HRS 241	NGC 4636	10.51	41.59	5.06	9.0	<7.02	− 3.94[c]	1, 3
VCC 345	NGC 4261	10.70	41.21	5.81	<8.45	<7.70	> − 2.71[d]	2, 3
VCC 1226	NGC 4472, M49	10.90	41.43	5.49	<7.90	<7.26	> − 2.50[d]	2, 3
VCC 1619	NGC 4550	9.72	39.78	5.41	<7.90	7.20	> − 2.57[d]	2, 3

Notes. [a]References: (1) Smith et al. (2012); (2) di Serego Alighieri et al. (2013); (3) O'Sullivan et al. (2001).
[b]Adopted from Ref. 1. Ref. 2 gives 5.30 with the same mass absorption coefficient.
[c]The upper limit of H_2 mass is used, but this does not affect the estimated dust-to-gas ratio since the gas mass is dominated by H I gas mass.
[d]We use the upper limits of gas mass to derive the lower limits of dust-to-gas ratio.

growth (time is measured from the onset of grain growth). We show the total to selective extinction $R_\lambda \equiv A_\lambda/E(B-V) = A_\lambda/(A_B - A_V)$ (the wavelengths at the B and V bands are 0.44 and 0.55 μm, respectively), which is sensitive to the extinction curve slope around these two optical bands. The observational extinction curves for a sample of elliptical galaxies are taken from Patil et al. (2007): we only chose those galaxies that are classified as elliptical galaxies and have extinction data at all bands (B, V, R, and I).

We observe in Fig. 9 that the initial extinction curves before grain growth tend to overproduce R_λ since they are too flat [i.e. the colour excess $E(B-V)$ is small] compared with the observed extinction curves. They are also flatter than the Milky Way extinction curve, which has $R_V \simeq 3.1$ (e.g. Draine 2003), because of the deficiency of small grains (note that the grain size distribution after sputtering in Fig. 3 is $\propto a^{-2.5}$ while the Milky Way extinction curve is fitted by a grain size distribution $\propto a^{-3.5}$; MRN). After grain growth by accretion takes place, the extinction curve becomes steeper (or R_λ becomes smaller), which is consistent with the previous conclusion that grain growth by accretion steepens the extinction curve (Hirashita 2012). This is because, as explained in Section 4.2, accretion is much more efficient for smaller grains owing to their larger surface-to-volume ratio. Since R_λ is sensitive to the slope at B and V bands, the decrease of R_λ is significant if the abundance of grains with $a \lesssim \lambda/2\pi \simeq 0.07$ μm (for $\lambda = 0.44$ μm) increases (Bohren & Huffman 1983). This occurs up to 3×10^7 yr in Model a and 10^8 yr in Models b and c (Fig. 7). At 10^8 yr in Model a, almost all grains exceed 0.07 μm, leading to a significant increase of R_λ (or significant flattening of optical extinction curve), as seen in Fig. 9a.

It is not likely that we observe the extinction of single-aged clouds, but it is probable that we see a mixture of clouds with different ages at the same time. Considering this, it is interesting to point out that the observed extinction curves are just in the range explained by the grain growth. Sputtering in the hot gas tends to make the extinction curve too flat; the observed extinction curves favour subsequent grain processing that could form grains with $a \lesssim 0.07$ μm. Grain growth by accretion enhances the abundance of such 'small' grains.

The lognormal grain size distribution of AGB dust produces completely flat extinction curve at $\lambda \lesssim 1$ μm, even if we consider accretion. Since $E(B-V)$ is slightly negative (i.e. R_λ is negative and $|R_\lambda|$ is extremely large), the results cannot be displayed. Therefore, the lognormal model does not fit the observed extinction curve unless there is an extra mechanism of small grain production (see Section 5.3).

5.3 Shattering?

Hirashita & Yan (2009) also showed that the dust grains may be shattered in the warm ($\sim 10^4$ K) diffuse medium in the Galactic environment (see also Yan et al. 2004). If some fraction of the gas remains to be diffuse after cooling of the hot gas and turbulent velocity is as high as $\gtrsim 1$ km s^{-1}, grains may be shattered. This would enhance the abundance of small grains and would steepen the extinction curve. If the dust is processed by shattering before being included in the cold dense medium, the total surface area of the dust is enhanced, resulting in more efficient dust growth by accretion and further steepening of the extinction curve. Therefore, the presence of shattering would enhance our conclusion that dust processing after cooling is a key to understanding the dust abundance and the steepness of extinction curves in elliptical galaxies. However, in a high-pressure environment in the central part of elliptical galaxies, such a diffuse warm medium is not realized as an equilibrium state (Wolfire et al. 1995). Therefore, a dynamical model is necessary to treat this intermediate temperature range $\sim 10^4$ K, which is left for the future work.

5.4 Implication of the internal origin of dust

We have shown that accretion in the cold medium is a viable mechanism of solving the discrepancy between the expected dust abundance after sputtering and the observed one in elliptical galaxies. Moreover, the steepening of extinction curves by accretion in the cooled medium is favoured in terms of the steepness of observed extinction curves. Although we do not intend to argue that all the dust in elliptical galaxies are of internal origin, it is worth noting that more careful consideration is necessary before resorting to the external origin of elliptical galaxy dust.

Even if accretion is the most dominant dust source, the dust supplied by AGB stars works as seeds for accretion. Therefore, the dust supply by AGB stars is still important in obtaining the thorough understanding of the life-cycle of dust in elliptical galaxies. The present-day mass loss rate of AGB stars in elliptical galaxies can be constrained by the mid-infrared emission emitted by AGB dust (e.g. Athey et al. 2002). Villaume, Conroy & Johnson (2015) demonstrated that circumstellar dust around AGB stars can account for the mid-infrared (8–24 μm) flux in some early-type galaxies. Spectral synthesis models including mid-infrared emission of AGB dust such as those presented in Villaume et al. (2015) can be used to constrain the dust yield of a population of AGB stars in a galaxy

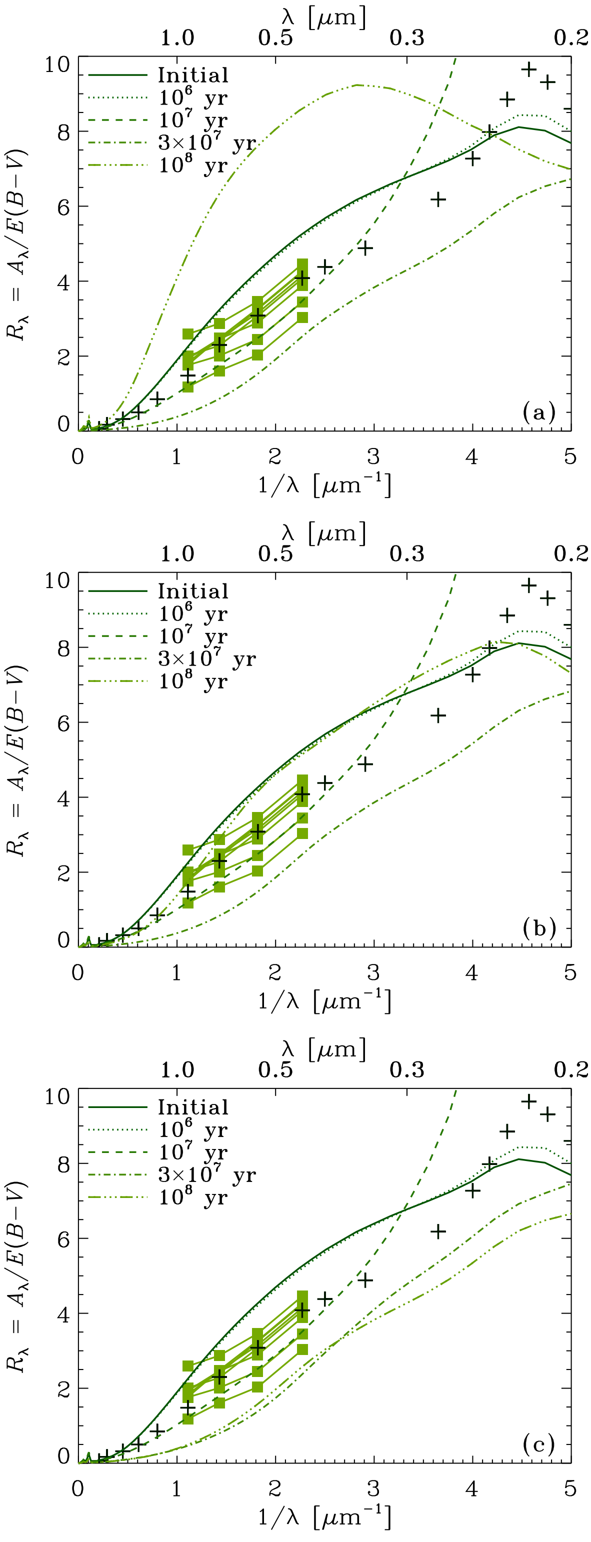

Figure 9. Extinction curves normalized to $E(B-V)$. Panels (a), (b), and (c) show the results for Models a, b, and c, respectively. The solid curve shows the extinction curves at the final stage of gas cooling in Fig. 3, which corresponds to the extinction curve at the onset of grain growth in the cold medium. The dotted, dashed, dot–dashed, triple-dot–dashed lines present the extinction curves at 10^6, 10^7, 3×10^7, and 10^8 yr after the onset of grain growth. The squares connected by the solid line are observational data for an elliptical galaxy sample in Patil et al. (2007). The crosses show the Milky Way extinction curve as a reference.

using observed dust emission. This is a crucial component for understanding whether an internal origin is a plausible explanation for the observed dust in early-type galaxies.

Theoretical dust yields of AGB stars are also tested by observations of nearby galaxies. Because of their proximity, the Magellanic Clouds provide us with an opportunity of detailed observational constraint on the dust formation in individual AGB stars (Srinivasan et al. 2009; Boyer et al. 2011; Srinivasan, Sargent & Meixner 2011; Riebel et al. 2012; Kemper 2013). According to Zhukovska & Henning (2013) and Schneider et al. (2014), the current models of dust production in AGB stars used or discussed in this paper (Ferrarotti & Gail 2006; Zhukovska et al. 2008; Ventura et al. 2014) are broadly consistent with the observed dust production rate by AGB stars in the Large Magellanic Cloud. However, Schneider et al. (2014) also mentioned that there is still a discrepancy between the model and observation for the Small Magellanic Cloud and that the metallicity dependence of the AGB dust yield is large. Since dust yields of solar-metallicity AGB stars have not been tested against observational data, observational studies on the dust formation by AGB stars in elliptical galaxies, which are, broadly speaking, solar-metallicity objects, give an important constraint on theoretical dust production models of AGB stars. The understanding of AGB dust yield is also crucial even for high-redshift galaxies, in which AGB stars may contribute to the dust enrichment (Valiante et al. 2009; Gall, Hjorth & Andersen 2011; Pipino et al. 2011).

6 CONCLUSION

We have reconsidered the origin of dust in elliptical galaxies, focusing on the internal origin; that is, the dust originates from the production by AGB stars within the galaxy. The evolution of grain size distribution is consistently solved along with the evolution of grain abundance by dust supply from AGB stars and dust destruction (sputtering) in the hot interstellar medium (ISM). We have confirmed that sputtering is so efficient that the dust abundance observed in the FIR cannot be explained. In addition, we have shown that cooling does not help to protect the dust from sputtering; rather, gas compression induced by cooling raises the sputtering rate so that the dust-to-gas ratio is decreased by cooling. Because of the rapid dust destruction, dust cooling has little influence on the thermal history of the cooling hot gas, unless the hot gas initially has a dust-to-gas ratio as high as $\sim$0.01 (i.e. comparable to the value in the Galactic cold ISM).

In the latter part of this paper, we have considered grain growth by the accretion of gas-phase metals in the cold clouds formed as a result of cooling of the hot gas, in order to examine a possibility that the dust abundance is increased or 'recovered' by this process. We find that, if accretion lasts longer than $10^7/(n_{\rm H}/10^3\ {\rm cm^{-3}})$ yr, which is shorter than the heating time-scale of AGN feedback, the dust-to-gas ratio can increase up to $\sim 10^{-3}$. Therefore, we do not necessarily need to resort to the external origin for the observed excessive dust abundance in elliptical galaxies, and we suggest dust growth by accretion in the cooled gas as a plausible explanation for the dust abundance. Since sputtering in the hot gas destroys small grains more efficiently than large grains, extinction curves after sputtering are too flat to explain the observed curves. The observed extinction curves are better explained by considering the effect of accretion, which enhances the abundance of small ($a \lesssim 0.07\ \mu$m) grains.

In summary, we conclude (i) that cooling does not protect the dust grains against sputtering, (ii) that dust cooling does not change the thermal history of the hot gas except for the case in which the hot gas initially has a dust-to-gas ratio as large as ~ 0.01, (iii) that the formation of cold dense gas as a result of cooling helps dust mass to increase through dust growth by the accretion of gas-phase metals, and (iv) that the observed extinction curves are consistent with this accretion scenario.

ACKNOWLEDGEMENTS

We thank C. Conroy and F. Kemper for valuable discussions. We also thank the anonymous referee for useful comments. HH is supported by the Ministry of Science and Technology (MoST) grant 102-2119-M-001-006-MY3. TN is supported in part by the JSPS Grant-in-Aid for Scientific Research (26400223).

REFERENCES

Asano R., Takeuchi T. T., Hirashita H., Inoue A. K., 2013a, Earth Planets Space, 65, 213
Asano R., Takeuchi T. T., Hirashita H., Nozawa T., 2013b, MNRAS, 432, 637
Athey A., Bregman J., Bregman J., Temi P., Sauvage M., 2002, ApJ, 571, 272
Bohren C. F., Huffman D. R., 1983, Absorption and Scattering of Light by Small Particles. Wiley, New York
Boyer M. L. et al., 2011, AJ, 142, 103
Caon N., Macchetto W. H., Turner E. L., 1992, ARA&A, 30, 499
Chokshi A., Tielens A. G. G. M., Hollenbach D., 1993, ApJ, 407, 806
Ciotti L., Ostriker J. P., 2001, ApJ, 551, 131
Dalgarno A., McCray R. A., 1972, ARA&A, 10, 375
Däppen W., 2000, in Cox N., ed., Allen's Astrophysical Quantities, 4th edn. Springer, New York
de Bennassuti M., Schneider R., Valiante R., Salvadori S., 2014, MNRAS, 445, 3039
di Serego Alighieri S. et al., 2013, A&A, 552, A8
Dominik C., Tielens A. G. G. M., 1997, ApJ, 480, 647
Draine B. T., 2003, ARA&A, 41, 241
Draine B. T., Salpeter E. E., 1979, ApJ, 231, 77
Dwek E., 1987, ApJ, 322, 812
Dwek E., 1998, ApJ, 501, 643
Fabian A. C., Johnstone R. M., Daines S. J., 1994, MNRAS, 271, 737
Ferrari F., Pastoriza M. G., Macchetto F., Caon N., 1999, A&AS, 136, 269
Ferrarotti A. S., Gail H.-P., 2006, A&A, 447, 553
Fitzpatrick E. L., Massa D., 2007, ApJ, 663, 320
Forbes D. A., 1991, MNRAS, 249, 779
Fujita Y. et al., 2013, PASJ, 65, L15
Gall C., Hjorth J., Andersen A. C., 2011, A&AR, 19, 43
Goudfrooij P., de Jong T., 1995, A&A, 298, 784
Goudfrooij P., Hansen L., Jørgensen H. E., Nørgaard-Nielsen H. U., 1994a, A&AS, 105, 341
Goudfrooij P., de Jong T., Hansen L., Nørgaard-Nielsen H. U., 1994b, MNRAS, 271, 833
Hirashita H., 1999, ApJ, 510, L99
Hirashita H., 2012, MNRAS, 422, 1263
Hirashita H., Kuo T.-M., 2011, MNRAS, 416, 1340
Hirashita H., Yan H., 2009, MNRAS, 394, 1061
Inoue A. K., 2011, Earth Planets Space, 63, 1027
Kaviraj S., Schawinski K., Silk J., Shabala S. S., 2011, MNRAS, 415, 3798
Kemper F., 2013, Earth Planets Space, 65, 223
Knapp G. R., Guhathakurta P., Kim D.-W., Jura M. A., 1989, ApJS, 70, 329
Kuo T.-M., Hirashita H., Zafar T., 2013, MNRAS, 436, 1238
Leeuw L. L., Sansom A. E., Robson E. I., Haas M., Kuno N., 2004, ApJ, 612, 837
Martini P., Dicken D., Storchi-Bergmann T., 2013, ApJ, 766, 121
Mathews W. G., Brighenti F., 1999, ApJ, 526, 114
Mathews W. G., Brighenti F., 2003, ApJ, 590, L5
Mathews W. G., Temi P. Brighenti F., Amblard A., 2013, ApJ, 768, 28
Mathis J. S., Rumpl W., Nordsieck K. H., 1977, ApJ, 217, 425 (MRN)
Mattsson L., Andersen A. C., 2012, MNRAS, 423, 38
Nozawa T., Fukugita M., 2013, ApJ, 770, 27
Nozawa T., Kozasa T., Habe A., 2006, ApJ, 648, 435
O'Sullivan E., Forbes D. A., Ponman T. J., 2001, MNRAS, 328, 461
Patil M. K., Pandey S. K., Sahu D. K., Kembhavi A., 2007, A&A, 461, 103
Pei Y. C., 1992, ApJ, 395, 130
Pellegrini S., Ciotti L., Ostriker J. P., 2012, ApJ, 744, 21
Pipino,A.,Fan X. L., Matteucci F., Calura F., Silva L., Granato G., Maiolino R., 2011, A&A, 525, A61
Raiteri C. M., Villata M., Navarro J. F., 1996, A&A, 315, 105
Rémy-Ruyer A. et al., 2014, A&A, 563, A31
Riebel D., Srinivasan S., Sargent B., Meixner M., 2012, ApJ, 753, 71
Schneider R., Valiante R., Ventura P., dell'Agli F., Di Criscienzo M., Hirashita H., Kemper F., 2014, MNRAS, 442, 1440
Seok J. Y., Koo B.-C., Hirashita H., 2015, ApJ, 807, 100
Smith M. W. L. et al., 2012, ApJ, 748, 123
Srinivasan S. et al., 2009, AJ, 137, 4810
Srinivasan S., Sargent B. A., Meixner M., 2011, A&A, 532, A54
Sutherland R. S., Dopita M. A., 1993, ApJS, 88, 253
Temi P., Brighenti F., Mathews W. G., Bregman J. D., 2004, ApJS, 151, 237
Temi P., Brighenti F., Mathews W. G., 2007, ApJ, 660, 1215
Tran H. D., Tsvetanov Z., Ford H. C., Davies J., Jaffe W., van den Bosch F. C., Rest A., 2001, AJ, 121, 2928
Tsai J. C., Mathews W. G., 1995, ApJ, 448, 84
Valentini M., Brighenti F., 2015, MNRAS, 448, 1979
Valiante R., Schneider R., Bianchi S., Andersen A. C., 2009, MNRAS, 397, 1661
van Dokkum P. G., Franx M., 1995, AJ, 110, 2027
Ventura P. et al., 2012, MNRAS, 424, 2345
Ventura P., Dell'Agli F., Schneider R., Di Criscienzo M., Rossi C., La Franca F., Gallerani S., Valiante R., 2014, MNRAS, 439, 977
Villaume A., Conroy C., Johnson B. D., 2015, ApJ, 806, 82
Voit G. M., Donahue M., 1995, ApJ, 452, 164
Voshchinnikov N. V., Hirashita H., 2014, MNRAS, 445, 301
Weingartner J. C., Draine B. T., 2001, ApJ, 548, 296
Werner N. et al., 2014, MNRAS, 439, 2291
Wiklind T., Combes F., Henkel C., 1995, A&A, 297, 643
Wolfire M. G., Hollenbach D., McKee C. F., Tielens A. G. G. M., Bakes E. L., 1995, ApJ, 443, 152
Yan H., Lazarian A., Draine B. T., 2004, ApJ, 616, 895
Yasuda Y., Kozasa T., 2012, ApJ, 745, 159
Zhukovska S., Henning T., 2013, A&A, 555, A99
Zhukovska S., Gail H.-P., Trieloff M., 2008, A&A, 479, 453

APPENDIX A: EVOLUTION OF GRAIN SIZE DISTRIBUTION UNDER A VARYING BACKGROUND GAS DENSITY

In the main text, we only concentrate on the single fluid element. If we explicitly treat the spatial variation of grain size distribution by denoting it as $n(a,\ \boldsymbol{x},\ t)$, where $\boldsymbol{x}$ is the spatial coordinate, the continuity equation corresponding to equation (1) is written as (see equation 37 in Tsai & Mathews 1995)

$$\left(\frac{\partial n}{\partial t}\right)_{a,\boldsymbol{x}} + \frac{\partial}{\partial a}(\dot{a}n) + \nabla\cdot(n\boldsymbol{u}) = S, \tag{A1}$$

where $\boldsymbol{u}$ is the velocity of the fluid, and $(\partial/\partial t)_{a,\boldsymbol{x}}$ is the partial derivative for time with fixed a and $\boldsymbol{x}$. The gas density follows the continuity equation written in Lagrangian (comoving) form as

$$\frac{\mathrm{d}\rho_{\mathrm{gas}}}{\mathrm{d}t} + \rho_{\mathrm{gas}}\nabla\cdot\boldsymbol{u} = 0. \tag{A2}$$

Eliminating $\nabla\cdot\boldsymbol{u}$ from equations (A1) and (A2), we obtain

$$\left(\frac{\partial n}{\partial t}\right)_{a,\boldsymbol{x}} + (\boldsymbol{u}\cdot\nabla)n - n\frac{1}{\rho_{\mathrm{gas}}}\frac{\mathrm{d}\rho_{\mathrm{gas}}}{\mathrm{d}t} + \frac{\partial}{\partial a}(\dot{a}n) = S. \tag{A3}$$

The first two terms are combined to obtain the Lagrangian derivative (with a fixed):

$$\left(\frac{\partial n}{\partial t}\right)_a - n\frac{1}{\rho_{\rm gas}}\frac{{\rm d}\rho_{\rm gas}}{{\rm d}t} + \frac{\partial}{\partial a}(\dot{a}n) = S. \tag{A4}$$

Thus, we obtain equation (1).

APPENDIX B: EQUILIBRIUM GRAIN SIZE DISTRIBUTION

As seen in the text, the sputtering time-scale is often much shorter than the cooling time-scale. Therefore, it is useful to discuss the equilibrium grain size distribution achieved by the balance between sputtering and supply from AGB stars (we neglect cooling here). Under this equilibrium condition, equation (1) is reduced to

$$\frac{\partial}{\partial a}[\dot{a}n(a)] = S(a), \tag{B1}$$

where we set all the time derivative terms as zero. Considering that $\lim_{a\to\infty} n(a) = 0$, the equilibrium grain size distribution is analytically written as

$$n(a) = \frac{1}{\dot{a}}\int_{\infty}^{a} S(a)\,{\rm d}a. \tag{B2}$$

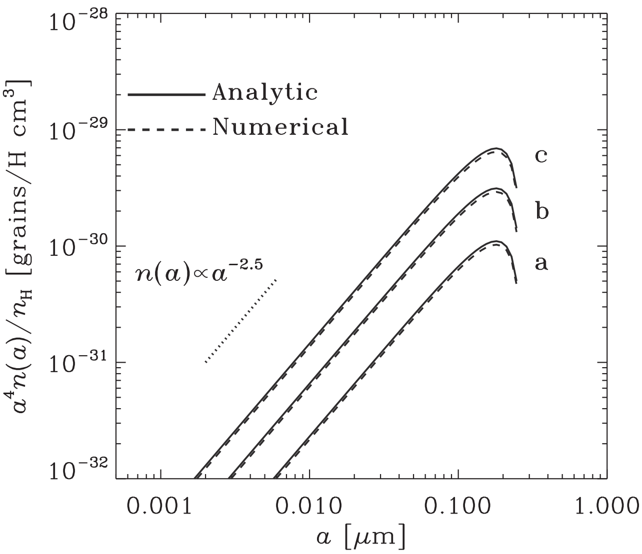

Figure B1. Equilibrium grain size distributions for Models a, b, and c (lower, middle and upper lines, respectively). We adopt the MRN grain size distribution for AGB dust and neglect cooling (i.e. the gas temperature and density are constant). The solid and dashed lines show the analytic and numerical solutions, respectively. For the numerical solution, we plot the grain size distributions at $t = 10^7$ yr, which is much longer than the sputtering time-scale.

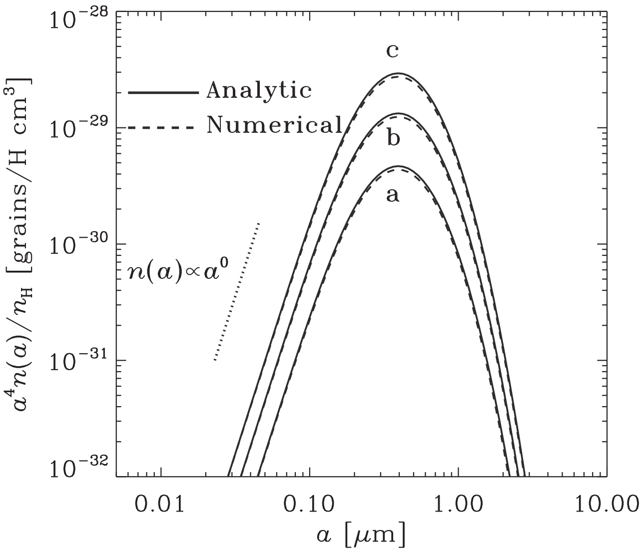

Figure B2. Same as Fig. B1 but for the lognormal grain size distribution for AGB dust.

If we adopt the MRN grain size distribution (equation 11), we obtain

$$n(a) = \frac{C\dot{\rho}_{\rm dust}}{-2.5\dot{a}}\left(a^{-2.5} - a_{\rm max}^{-2.5}\right), \tag{B3}$$

where $a_{\rm max} = 0.25\ \mu$m. Here, we have used equation (9) for S, and we can use equation (13) for $\dot{a}$ (note that $\dot{a}$ is negative). If a is significantly smaller than $a_{\rm max}$, $n(a) \propto a^{-2.5}$. The grain size distribution is less steep than that of AGB dust, since smaller grains are more easily destroyed than larger grains.

In Fig. B1, we show the above analytic solution. For comparison, we also show the numerical solution of equation (1) without cooling at $t = 10^7$ yr. Since the time-scales of sputtering and dust supply are much shorter than 10^7 yr, we expect that the grain size distribution has achieved the equilibrium at $t = 10^7$ yr. The analytic and numerical solutions are almost identical, which confirms that our numerical scheme correctly solves the evolution of grain size distribution by dust supply and sputtering. Moreover, as expected above, the slope of the equilibrium grain size distribution is described by a power law with an index of -2.5.

We also show the equilibrium solution for the lognormal grain size distribution of AGB dust in Fig. B2. The numerical solution is produced in the same way as above; that is, we used the result at $t = 10^7$ yr with cooling neglected. The 'analytical' solution is obtained by numerically integrate equation (B2). We confirm that the numerical results reproduce the analytical results well. At $a \ll a_0 = 0.1\ \mu$m (the central radius of the lognormal distribution), $n(a) =$ constant since $S(a)$ drops exponentially in that grain radius range. We can confirm this in Fig. B2.

This paper has been typeset from a TEX/LATEX file prepared by the author.